JAISCR, 2012, Vol. 2, No. 4, pp. 331 – 342

INTELLIGENT SENSING AND MONITORING – RESPIRATORY MOTION PREDICTION FOR TUMOR FOLLOWING RADIOTHERAPY

Kei Ichiji[1], Noriyasu Homma[2], Masao Sakai[3], Ivo Bukovsky[4],
Xiaoyong Zhang[5], Makoto Osanai[5], Makoto Abe[6], Norihiro Sugita[6], Makoto Yoshizawa[7]

[1]*Graduate School of Engineering, Tohoku University, Sendai, Japan*

[2]*Tohoku University Graduate School of Medicine, Sendai, Japan*

[3]*Center for Information Technology in Education, Tohoku University, Japan*

[4]*Czech Technical University in Prague, Prague, Czech Republic*

[5]*Tohoku University Graduate School of Medicine, Sendai, Japan*

[6]*Graduate School of Engineering, Tohoku University, Sendai, Japan*

[7]*Cyberscience Center, Tohoku University, Sendai, Japan*

Abstract

This paper presents a medical application of the intelligent sensing and monitoring, a new lung tumor motion prediction method for tumor following radiation therapy. An essential core of the method is accurate estimation of complex fluctuation of time-varying periodical nature of lung tumor motion. Such estimation is achieved by using a novel multiple time-varying seasonal autoregressive (TVSAR) model in which several windows of different time-lengths are used to calculate correlation based fluctuation of periodic nature in the motion. The proposed method provides the prediction as a combination of those based on different window lengths. Multiple regression (MR), multilayer perceptron (MLP) and support vector regression (SVR) are used to combine and the prediction performances are evaluated by using clinical lung tumor motion. The proposed methods with the combined predictions showed high accurate prediction and are superior to the single different predictions. The average errors of MR, MLP, and SVR were 0.8455, 0.8507, and 0.7530 mm at 0.5 s ahead, respectively. The results are clinically sufficient and thus clearly demonstrate that the proposed TVSAR with an appropriate combination method is useful for improving the prediction performance.

1 Introduction

Medical applications can be a good challenge for the merge of computational intelligence and sensor technology. Indeed, intelligent sensing of useful pieces of medical information to diagnose patients and optimizing medical instruments to achieve the best treatment effect are needed in such medical applications, just to name but a few.

In this paper, we focus on an intelligent prediction of lung tumor motion for radiotherapy in which continuously irradiating a sufficient dose to tumor yields a better therapeutic effect and can shorten the

duration of treatment. It is also required to decrease an adverse effect by avoiding irradiation to normal tissues located around the target tumor.

Observing the target tumor location and properly planning the irradiated field are necessary for accurate, sufficient, and continuous irradiation. Such desirable irradiation has already been used and reported good treatment results which are even equal to surgery [1]. However, activities of internal organs such as lung and heart move a tumor during the treatment fraction, and the tumor motion makes it difficult to achieve precise setup and accurate continuous irradiation. Therefore, pre-planned static irradiation area may not suitably cover the moving target tumor. In addition, we cannot irradiate sufficient therapeutic dose to patient because the therapeutic dose may also cover the surrounding healthy tissues by the internal organ motion.

Recently, a basic concept of tumor-following radiation therapy (TFRT) using real-time image guided techniques has been proposed for continuous irradiation to moving tumor such as lung tumor [2]. In TFRT, the radiation beam is repositioned and reshaped to adapt to the lung tumor motion and the deformation in real-time. The irradiated area can suitably be limited around the target tumor by beam repositioning and reshaping. Thus, the exposure of normal tissues to the dose can be decreased.

However, there are some challenges to be solved for clinical use of TFRT, such as:

1. Real-time measurement for tumor position and shape.

2. Compensation of inherent latencies in radiation device.

The first technique, measurement of the tumor location can be achieved by using an X-ray fluoroscopic imaging system and implanted fiducial markers [3]. However, real-time beam-repositioning has not been developed yet because current radiotherapy machines have mechanical and computational time delays of up to about 1 s for controlling irradiation field and image processing. The latency definitely affects badly on the irradiation accuracy [4], and thus must be compensated.

Typical solution for compensation of the latency is to predict the lung tumor motion [5, 13, 7, 8]. Among them, a time-varying seasonal autoregressive (TVSAR) is an natural extension of the general seasonal AR model to take into account of a time varying nature of the respiratory motion, and can achieve the best performance of highly accurate prediction of less than 1 mm at 1 s ahead. We have also reported that TVSAR can change the sensitivities to follow the time varying nature and the better prediction performance can be achieved by the better sensitivities [11]. In addition, the experimental results have suggested that more appropriate use of the sensitivities can further improve the prediction performance.

In this paper, we further investigate the use of the sensitivities of TVSAR predictions and propose a new prediction method to improve the prediction performance for TFRT. The proposed method is composed of two parts:

1. A part consists of several predictors with different settings

2. A part for combining the several predictions

The predictors to be combined produce each prediction with different sensitivities and each can be superior to others at specific situation. To obtain the better prediction performance, the second part intelligently combines those different predictions based on the sensitivities.

The rest of this paper consists of as follows. First we explain a lung tumor motion used for this study in section II. Then seasonal prediction methods including the proposed method are described in section III. Section IV shows the superiority of the proposed method on prediction performance. Conclusions are provided in the last section.

2 Target Time Series: Lung Tumor Motion

The three-dimensional time series of the patient's lung tumor motion were obtained at Hokkaido University [3] and relatively-clean three data sets are used for this study (i.e., the data are composed of regularly breathing). The time series of tumor location was observed as a location of the golden fiducial marker implanted into around the tumor, by using a kV X-ray fluoroscopic system with sampling frequency 30 Hz. Observational

noise and outliers were preliminarily reduced by using statistical and low-pass filters.

Let us henceforth consider a time series for each spatial dimension of left to right (LR), cephalocaudal (CC), and anteroposterior (AP) axes as follows.

$$\{y(1), y(2), \cdots, y(t), \cdots\} \tag{1}$$

where $\{y(t)\}$ (mm) denotes a tumor coordinate at discrete time t.

Figure 1 shows the three data sets of the lung tumor motion. As is clear from this figure, the motion has a periodical nature mainly caused by patient's respiration. Therefore, we can also consider that the tumor motion is a kind of periodical function of time. Then a sinusoidal periodic model of the time varying nature of the motion can be given as

$$y(t) = A(t)\cos\vartheta(t) \tag{2}$$

where $A(t)$ and $\vartheta(t)$ are instantaneous amplitude and instantaneous phase at time t, respectively. Note that, a temporal differentiation of the phase is not constant, and changes with time in the model. (i.e., $d\vartheta(t)/dt \neq$ const.).

Such quasi-periodical nature of the motion can be confirmed by observing the period of the time series. For example, period $s(t)$ as time interval between a peak and next peak differs each other even if the amplitude variation $A(t)$ is sufficiently small as shown in figure 2. An average $\bar{s}$ of the period is about 90 (3 s) for the three data sets used in this paper.

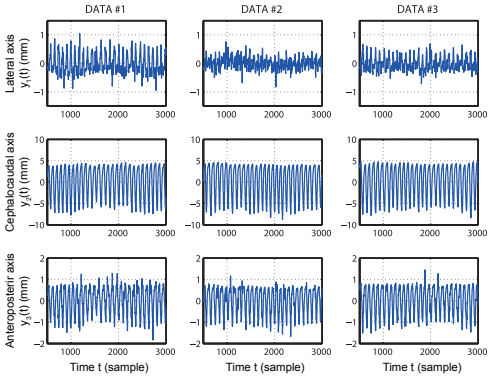

Figure 1. Three clinical data of 3D time series of lung tumor motion for different treatment fractions. These tumor motions have a quasi-periodical nature of the average period $\bar{s} = 90$ (3 s).

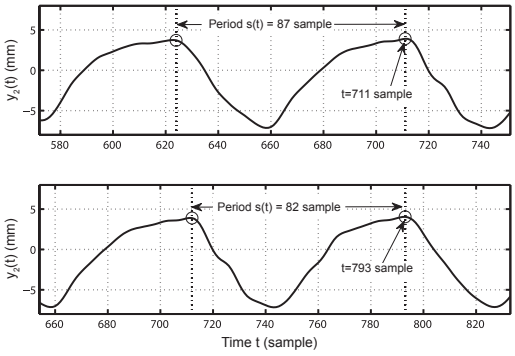

Figure 2. An example of time varying period $s_2(t)$ obtained as intervals among peaks of cephalocaudal motion $y_2(t)$ of DATA #1. Peak to peak periods are $s_2(t) = 87$ at time $t = 711$ and $s_2(t) = 82$ at time $t = 793$, respectively.

3 Prediction Methods

In this section, prediction methods based on a seasonal time series model are described. First we introduce a traditional seasonal method and explain its limitations on prediction of the lung tumor motion. Then, the seasonal prediction method is extended to take into account a time-varying nature of the periodical motion. At last, we propose a new prediction system by using the extended seasonal prediction methods.

3.1 Seasonal Prediction Method: Seasonal Autoregressive Model

Seasonal autoregressive integrated moving-average (SARIMA) model is a general expression of the time series which varies periodically (i.e., a periodical function of time such as trigonometric function).

The SARIMA model of the time series $\{x(0), x(1), \ldots, x(t)\}$ with period s can be expressed as follows.

$$\phi(B)\Phi(B^s)(1-B)^d(1-B^s)^D x(t) = \theta(B)\Theta(B^s)\varepsilon(t) \tag{3}$$

where d and D are respectively the order of local and seasonal integrated components, $\varepsilon(t)$ is the Gaussian noise of which mean and variance are 0 and σ^2, respectively, and B is a delay operator de-

fined by

$$B^k x(t) = x(t-k),\ k = 1,2,\ldots \tag{4}$$

Then, each components of the SARIMA model are given as follows.

$$\text{Autoregressive: } \phi(z) = 1 - \phi_1 z - \cdots - \phi_p z^p \tag{5}$$

$$\text{Moving-average: } \theta(z) = 1 + \theta_1 z + \cdots + \theta_q z^q \tag{6}$$

$$\text{Seasonal AR: } \Phi(z) = 1 - \Phi_1 z - \cdots - \Phi_P z^P \tag{7}$$

$$\text{Seasonal MA: } \Theta(z) = 1 - \Theta_1 z + \cdots + \Theta_Q z^Q \tag{8}$$

where p, q, P and Q are the orders of four components in (5)-(8) respectively.

The SARIMA model can express various periodical time series by designing the model settings. In the followings, let us consider only the seasonal autoregressive (SAR) component to avoid the over fitting problem and to simplify the explanation of the prediction method. That is, let $p = q = Q = d = D = 0$ in (3), then for this special case, we can obtain the following equation of seasonal autoregressive (SAR) model for the time series $y(t)$.

$$y(t) = \varepsilon(t) + \sum_{\rho=1}^{P} \Phi_\rho \cdot y(t - \rho \times s) \tag{9}$$

where P is the order of the SAR components, Φ_ρ are the SAR coefficients, and s are the constant period of the time series.

Then, to substitute $t+h$ for t, the prediction equation by using (9) can be given by

$$\hat{y}(t+h|t) = \sum_{\rho=1}^{P} \Phi_\rho \cdot y(t + h - \rho \times s) \tag{10}$$

where $\hat{y}(t+h|t)$ is the predicted value at future time $t+h$ with h samples ahead of current time t, and the term $h - \rho \times s$ must be not longer than 0 for composing the prediction by using only past observations.

The equations (9) and (10) indicate that an essential core of the general SAR depends on an assumption that each values of the same phase highly correlate each other. For example, periodical functions such as cosine wave $y(t) = \cos(2\pi f t)$ of frequency $f = 1/s$ as shown in figure 3 can be perfectly predicted by using (10) with period $s = 100$.

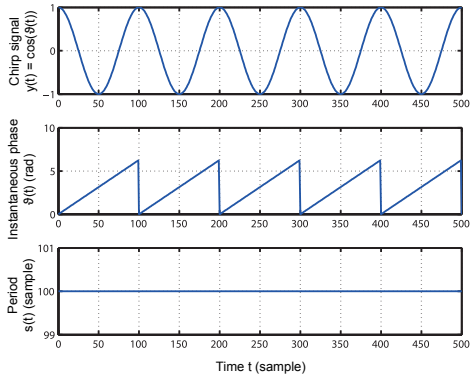

Figure 3. Cosine wave $y(t) = \cos(\vartheta(t))$ with constant period s. Instantaneous phase $\vartheta(t)$ is constantly changed. Such time series can be perfectly predicted by using the general SAR in (10).

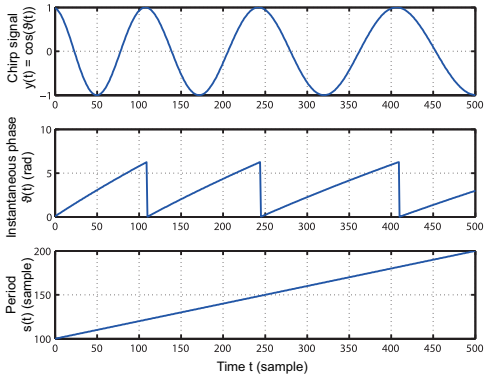

Figure 4. A chirp signal $y(t)$ generated by using time-varying period $s(t)$. The general SAR in (10) cannot predict this time series accurately. On the other hand, time-varying SAR based prediction in (20) can provide a predictability of this time series.

On the other hand, the general SAR model has a limitation that it cannot express accurately a seasonal time series with a time-varying period $s(t)$. Also, even if the time-varying period $s(t)$ is known instead of the constant period s, the phase $\vartheta(t_c)$ at the current time t_c and the past phase $\vartheta(t - \rho \times s(t))$ do not always correspond to each other. For example, if the target time series is a chirp signal $y(t)$ in which the period changes with time as shown in figure 4, the general SAR based equations (9) and (10) are not applicable to the target time series. That is, if the current time is $t_c = 350$, then the current amplitude, phase and period are $y(t_c) = -0.4315$, $\vartheta(t_c) = 4.1537$ rad and $s(t_c) = 170$, respectively.

However, the equation (9) for the order $\rho = 1$ and 2 provides improper values as $y(t_c - \rho \times s(t_c)) = -0.9220$ and 0.7077 and $\vartheta(t_c - \rho \times s(t_c)) = 3.4313$ and 0.6843 [rad], respectively because the term $\rho \times s$ in (9) and (10) are not references to the corresponding phase.

In addition, the lung tumor motion has the time varying nature as already shown in figure 2. Therefore, the general SAR is unusable to accurately predict the lung tumor motion [9].

3.2 Extended Seasonal Prediction Method: Time-varying SAR (TVSAR)

To overcome the limitation of the conventional SAR, we have proposed a time-varying SAR (TVSAR) model for prediction of the lung tumor motion [7, 8]. The TVSAR equation corresponding to (9) can be expressed as

$$y(t) = \varepsilon(t) + \sum_{\rho=1}^{P} \Phi_\rho \cdot y(t - r_\rho(t)). \qquad (11)$$

where $r_\rho(t)$ are reference intervals of the ρth order at time t.

The reference intervals $r_\rho(t)$ can be defined as a time interval between the current time and the corresponding past time which has the same phase to the current one. In other words, if an instantaneous phase $\vartheta(t)$ of the time series is given, the reference intervals can be defined as follows.

$$r_\rho(t) = \arg\min_{k>0} |\vartheta(t) - 2\rho\pi - \vartheta(t-k)| \qquad (12)$$

Also, if the period is a constant, the reference intervals can be expressed by

$$r_\rho(t) = \rho \times s, \text{ if } \frac{d\vartheta(t)}{dt} = \frac{2\pi}{s}. \qquad (13)$$

Note that, the constant reference interval shown by (13) corresponds to that used in the general SAR equations of (9) and (10).

Then, an ideal prediction equation of the time-varying SAR is expressed by substituting $t + h$ for t as follows.

$$\hat{y}(t+h|t) = \sum_{\rho=1}^{P} \Phi_\rho \cdot y(t + h - r_\rho(t+h)) \qquad (14)$$

where the term $h - r_\rho(t+h) \leq 0$.

Note that, in (14), we have to know the reference interval at h samples ahead future, but it is unknown in practice. In this case, we need to estimate it. The estimation method will be explained in the next section.

3.3 Online Estimation of Reference Intervals: Correlation analysis-based technique

In TVSAR, the reference intervals $r_\rho(t)$ are an important factor to predict the lung tumor motion accurately, and must be estimated on-line. In this study, a correlation analysis is adopted to estimate the reference intervals.

The correlation analysis based estimation procedure of the reference intervals is as follows.

1. Calculate a correlation function between two time series subsets of current values and past values. The correlation function is given as follows.

$$\gamma(t,k) = \frac{1}{w(t)} \sum_{j=0}^{w(t)-1} y(t-j) \cdot y(t-k-j) \qquad (15)$$

where $w(t)$ is a length of a rectangular window. The window length is updated at each time by using the latest estimation of the first order reference interval as

$$w(t) = \check{r}_1(t-1). \qquad (16)$$

2. The estimated reference intervals $\check{r}_\rho(t)$ can be obtained by the intervals between $k = 0$ and the peak intervals of the correlation function $\gamma(t,k)$ corresponded to each seasonal order ρ:

$$\check{r}_\rho(t) = \arg \max_{\check{r}_\rho(t-1)-l \leq k \leq \check{r}_\rho(t-1)+l} \gamma(t,k) \qquad (17)$$

where l defines the search area for the peak of $\gamma(t,k)$.

The initial condition is defined as follows.

$$\check{r}_\rho(1) = \rho \times \bar{s}, \qquad (18)$$

$$w(1) = \check{r}_1(1) \qquad (19)$$

where $\bar{s}$ is the average of pre-observed time varying periods of the time series. $\bar{s} = 90$ was used for this study.

An example of the correlation function and estimated reference intervals is shown in figure 5. As is clear from this figure, reference intervals of lung tumor motion intricately change with time evolution.

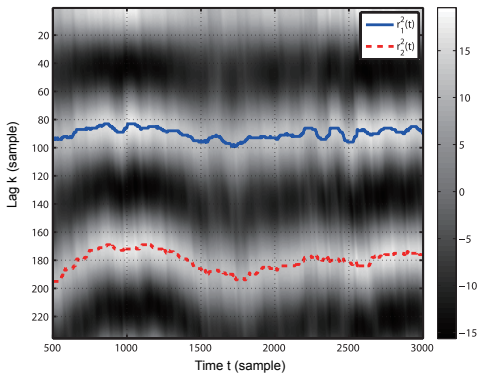

Figure 5. An example of the correlation function $\gamma(t,k), i = 2$ and estimeted reference intervals $\check{r}_\rho(t), \rho = 1,2$ for cephalocaudal-axis of DATA #1.

We can now estimate the reference intervals, but we need future value of them for (14). According to our previous study, prediction of these reference intervals is difficult [10], so $r_\rho(t+h)$ cannot be directly used for the prediction in (14). As a realistic way, we simply extrapolated $r_\rho(t+h)$ from the current estimate $\check{r}_\rho(t)$ with zero-order hold: $\hat{r}_\rho(t+h|t) = \check{r}_\rho(t)$. Then, (14) can be rewritten as

$$\hat{y}(t+h|t) = \sum_{\rho=1}^{P} \Phi_\rho \cdot y(t+h-\check{r}_\rho(t)). \tag{20}$$

This special prediction equation of TVSAR can achieve a higher accurate prediction compared to the general SAR of (10) [7][8].

3.4 Prediction Performance by using Correlation Analysis with Several Window Lengths

The correlation analysis based method requires a window length to be involved in (17) as a designable parameter. Then, it is considered that the correlation function with shorter window length can follow changes of reference intervals more quickly, but at the same time, is more sensitive to noise. On the other hand, the correlation function with longer window length is more robust to noise, however, it can only follow slower changes of the reference interval.

For discussing the effect of the window length, let us try to predict clinical lung tumor motion by using several window lengths. Several window lengths are used instead of (16) as follows.

$$w_n(t) = \alpha_n \cdot \check{r}_{n,1}(t-1) \tag{21}$$

where α_n are constant coefficients to define window lengths, $n = 1,2,\ldots$ are indexes, and $\check{r}_{n,1}(t)$ is the first order reference interval that estimated by using the correlation function with $w_n(t-1)$. The window length coefficients were empirically set as $\alpha_n = 0.5, 1$ and1.5 for $n = 1,2$ and 3, respectively.

The prediction equation of each window length $w_n^i(t)$ can be given by using $\check{r}_{n,\rho}(t)$ as

$$\hat{y}_n(t+h|t) = \sum_{\rho=1}^{P} \Phi_{n,\rho} \cdot y(t+h-\check{r}_{n,\rho}(t)). \tag{22}$$

In this study, to avoid the over fitting problem, the SAR coefficients and the SAR order are empirically set as $\Phi_{n,\rho} = 1/P$ and $P = 2$, respectively.

As a benchmark method, zero order hold (ZOH) is also tested. The prediction of ZOH equation is as follows.

$$\hat{y}_{\mathrm{ZOH}}(t+h|t) = y(t) \tag{23}$$

As is clear from the prediction equation, ZOH assumes that future values at any h will be same as the latest observed value. Also the result of ZOH corresponds to the case of tumor-following irradiation without compensation of the system latency.

3.4.1 Evaluation metric for prediction performance

Mean absolute error (MAE) between real and predicted values is used as a prediction performance measure. MAE is calculated as follows.

$$\mathrm{MAE}(h) = \frac{1}{t_e - t_s} \sum_{t=t_s}^{t_e} |e(t+h,h)| \tag{24}$$

where $t_e = 3000$ and $t_s = 500$ are the upper and the lower bounds of evaluation interval respectively, and $e(t,h)$ is the Euclidean distance between real and predicted values defined as follows.

$$e(t+h,h) = \sqrt{\sum_i (\hat{y}_i(t+h|t) - y_i(t+h))^2} \tag{25}$$

Here $i = \{\text{LR, CC, and AP}\}$ are indices for three-dimensional space and corresponding to lateral-, cephalocaudal-, and anteroposterior-axes, respectively.

Note that, the Euclidean error and their MAE both are functions of prediction horizon h.

3.4.2 Prediction performances of each model

TVSAR with the correlation analysis by using each of window lengths $\alpha_1 = 0.5, \alpha_2 = 1.0$ and $\alpha_3 = 1.5$, and zero-order hold (ZOH) are tested on each of data sets shown in Figure 1. Then evaluation results, MAEs as functions of prediction horizon, are shown in figure 6.

According to this figure, the best performance for each prediction horizon was achieved by the different prediction methods. For example, the least MAE for $1 \leq h \leq 2$ ahead prediction is clearly achieved by ZOH. It is not a surprise because the values temporally close to each other are similar to each other in amplitude. However, MAE of ZOH rapidly increases with prediction horizon h. At $h = 30$, MAE of ZOH became over 5 mm. MAE of ZOH indicates the importance of the prediction.

For short-term prediction at $3 \leq h \leq 9$, TVSAR with window length coefficient $\alpha_1 = 0.5$ is superior to other predictions, but, MAE of $\alpha_2 = 1$ is the least for $10 \leq h \leq 28$. Then, TVSAR with $\alpha_3 = 1.5$ is barely the least MAE for $28 \leq h \leq 30$ and almost similar to $\alpha_2 = 1$ for long-term prediction.

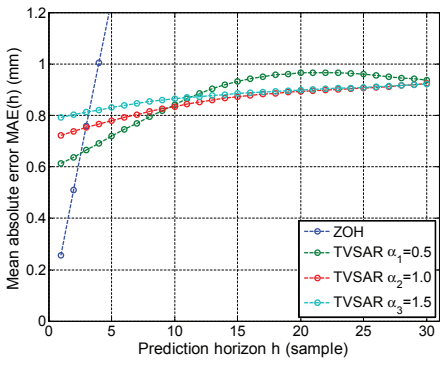

Figure 6. Mean absolute errors (MAEs) of TVSAR with the correlation analysis by using each of window lengths $\alpha_1 = 0.5, \alpha_2 = 1.0$ and $\alpha_3 = 1.5$, and zero-order hold (ZOH).

3.5 Proposed System: Combining Different Predictions

It has been seen that reference intervals calculated by different window lengths (coefficients) have useful pieces of information for the specific samples ahead predictions. In addition, even ZOH can be useful for very short-term prediction. We will then try to combine them to achieve better prediction performance.

The proposed system is composed of two parts:

- Prediction part: Predict the tumor motion by using several prediction models.
- Combination part: Combine the different predicted values provided by the prediction part.

Final prediction (i.e., the system output) can be expressed as follows.

$$\hat{y}_c(t+h|t) = f_h\left(\hat{y}(t+h|t)\right) \tag{26}$$

Here $\hat{y}_c(t+h|t)$ is the combined prediction, $f_h(\cdot)$ is a combining function for specific prediction horizon h, and $\hat{y}(t+h|t)$ is an input vector (i.e., output from the prediction part), respectively.

Figure 7 shows schematic diagram of the proposed prediction system. In this study, the input vector $\hat{y}(t+h|t)$ consists of N predicted values of TVSAR with several window lengths given by (22), and prediction value of zero-order hold given as $\hat{y}_{\text{ZOH}}(t+h|t) = y(t)$. Note that the multiple regression shown in this figure is just an example of the combination part. Then, following methodologies are used as a combining function $f_h(\cdot)$ to produce the predicted values.

3.5.1 Multiple Regression (MR)

A simple combination of the multiple regression method can be defined by

$$f_h\left(\hat{y}(t+h|t)\right) = \beta_0 + \beta_{N+1} \cdot \hat{y}_{\text{ZOH}}(t+h|t) + \sum_{n=1}^{N} \beta_n \cdot \hat{y}_n(t+h|t) \tag{27}$$

where $\beta_n, n = 0, 1, \ldots, N+1$ are regression coefficients. The coefficients are estimated to reduce the prediction error by using the least-squares technique [17].

3.5.2 Multilayer perceptron (MLP)

Multilayer perceptron (MLP) is adopted as a nonlinear combining function. In this study, we have empirically adopted three layers feed forward network with 16 hidden neural units. Each prediction by TVSAR models and the zero-order hold prediction are given to MLP. The network is trained to minimize the mean squared prediction error by using Levenberg-Marquardt algorithm [16] and validated by using two-fold cross-validation technique [17] within training data set.

3.5.3 Support Vector Regression (SVR)

As another nonlinear approach, ε-Support Vector Regression (SVR) is also employed to the combination part. In this study, we used LibSVM by Chang et al.[12] for the implementation. The input variables same for MLP are fed to SVR, and the radial basis function was adopted as kernel function. Other settings are given as default values in the library.

4 Results

4.1 Experimental Setup and Validation

We have evaluated prediction performance of the proposed system by using three clinical data as shown in figure 1.

The time series $y(t)$ and predicted values $\hat{y}_n(t+h|t)$ of $501 \leq t \leq 1750$ are used for training the combining functions. That is, the combining functions are adjusted to adapt to the first half of each treatment fraction. Note that such adaptation process can be adopted before the treatment time in clinical.

Mean absolute error (MAE) in (24) with $\{t_s, t_e\} = \{501, 1750\}$ was used as an evaluation index for each prediction methods among three data sets.

Figure 8 shows the average MAE by the proposed prediction system with three combination approaches among the data sets of the first half. MAEs of the single TVSAR predictions with $\alpha_n = \{0.5, 1, 1.5\}$ and ZOH are also shown for comparison. As is clear from this figure, the proposed system with the MLP and SVR combinations achieved the best and the second best MAEs for prediction horizons $1 \leq h \leq 30$ (0.033 s to 1.000 s) respectively. MAE of MR is also better than each single TVSAR and ZOH. These results indicates that these combinations were well adapted to the first half of each data set. Overall, these results suggest the effectiveness of the proposed combination approaches.

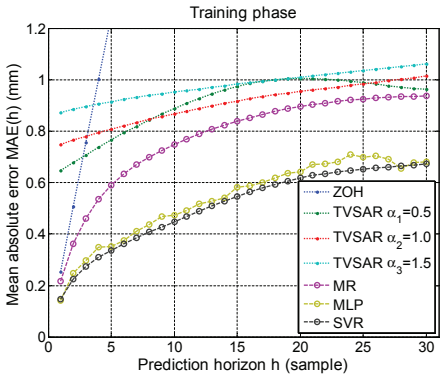

Figure 8. Mean absolute error MAE(h) of several prediction methods for confirmation of the adjustment of MR, MLP, and SVR combinations. Each curve means each method's average among three data sets of the first half ($\{t_s, t_e\} = \{501, 1750\}$).

4.2 Evaluation of Prediction Performance

The three combination methods were also tested on the last half ($y(t)$ of $1751 \leq t \leq 3000$) of each data set. MAE with $\{t_s, t_e\} = \{1751, 3000\}$ was used again.

Figure 9 and Table 1 show the performance by the proposed three combination methods and each of predictions combined. As is clear from this figure, all the proposed combination techniques achieved less MAEs than any single prediction for short- to mid-term (about $1 \leq h \leq 30$). Especially, the MAEs of MR and SVR are almost less than the single predictions for all the prediction horizon h. Therefore, to combine several different predictions is basically useful to improve the prediction performance.

The proposed method with SVR combination achieved the least MAE widely for prediction horizons on both halves of the data sets. This result suggests that there is a complex nonlinear relation among the different predictions and the true future value. Moreover, it can be considered that such

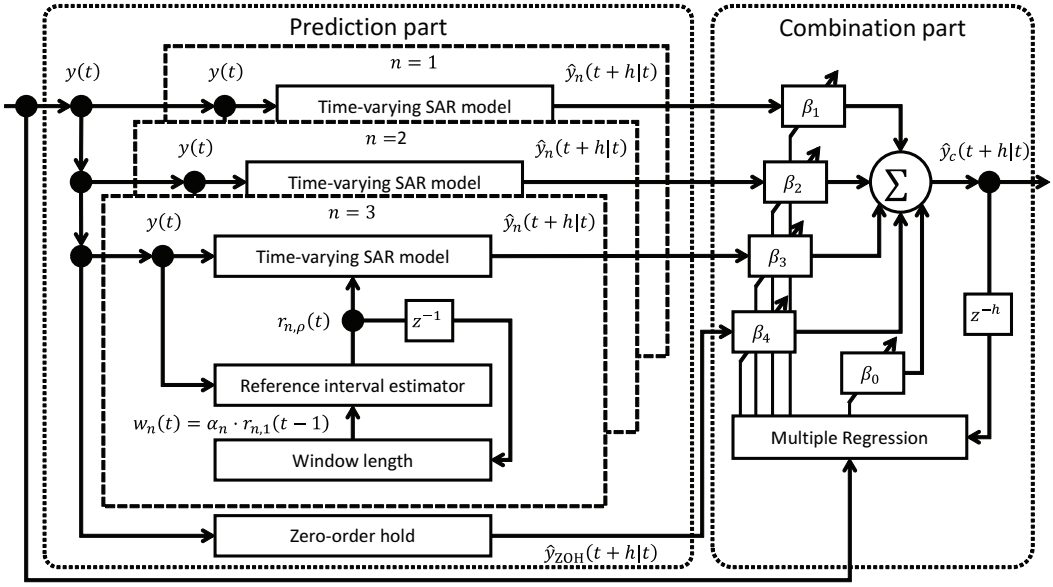

Figure 7. Schematic diagram of the proposed prediction system. The system is composed of two parts of that (a) several prediction models (3 TVSAR models and zero-order hold), and (b) combination part. Multiple regression is shown as an example of combination method.

nonlinear relation has a time varying nature. For example, on the first half of the data sets (i.e., training phase), nonlinear functions represented by MLP and SVR performed better MAEs than MAEs of other predictions. However, on the last half of the data sets, the MAE of MLP is not superior to the other methods for $h > 15$, and MLP was the worst for long-term prediction except for ZOH. Also the SVR combination indicated that the less superiority for long-term prediction. This can be due to the time varying nature of the nonlinear relation. In fact, the relation were changed for the last half ($1751 \leq t \leq 3000$): The error by the single TVSAR with $\alpha_3 = 1.5$ (red line) is the worst for the first half, but the it changes to the error by the single TVSAR with $\alpha_1 = 0.5$ (blue line) for $11 \leq h \leq 30$ of the last half. Thus, the combinations adjusted to only the relations on the first half could not perform well for the last half.

Investigating more detail relations and more efficient combination methods will be useful for further improvement. For example, exploring of appropriate parameter settings can help to improve the prediction performance. Also, the combinations were statically adjusted in this paper, but dynamic adaptation of the combinations may provide better prediction in some cases.

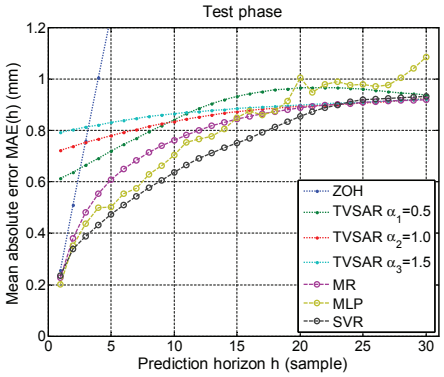

Figure 9. Mean absolute error MAE(h) with $\{t_s, t_e\} = \{1751, 3000\}$ for testing the prediction performances of the compared prediction methods.

4.3 Comparison with Other Prediction Methods

For comparison, we have tested two state-of-the-art prediction methods which were proposed for lung tumor motion.

4.3.1 Singular Spectrum Analysis based method

Demachi, et al. have applied a singular spectrum analysis (SSA) for lung tumor motion prediction[14, 15]. SSA is a the non-parametric

Table 1. Summary of prediction performance on test phase at several prediction horizons h.

Prediction methods		Avg. and std. of MAE among data sets $\mu_{\mathrm{MAE}} \pm \sigma_{\mathrm{MAE}}$ (mm)		
ZOH		0.256 ± 0.009	3.432 ± 0.143	5.810 ± 0.191
Single TVSAR	$\alpha_1 = 0.5$	0.613 ± 0.030	0.933 ± 0.033	0.940 ± 0.035
	$\alpha_2 = 1.0$	0.723 ± 0.015	0.874 ± 0.049	0.925 ± 0.076
	$\alpha_3 = 1.5$	0.794 ± 0.054	0.887 ± 0.088	0.922 ± 0.115
Proposed combinations	MR	0.226 ± 0.009	0.846 ± 0.020	0.920 ± 0.024
	MLP	0.201 ± 0.018	0.851 ± 0.124	1.087 ± 0.037
	SVR	0.235 ± 0.041	0.753 ± 0.009	0.934 ± 0.030
Prediction horizon h		1 (0.033 s)	15 (0.5 s)	30 (1 s)

time series analysis, and is based on singular value decomposition of the covariance matrix of target time series. Three designable parameters of SSA are length of training sample N, the dimension M of the covariance matrix, and τ for the dimension reduction, respectively. The predicted value $\hat{y}(t+1|t)$ is calculated as the weighted sum of the latest observed values. The weight coefficients are calculated by using dimension reduced singular vectors. Also, $h = 2,3,\ldots$ samples ahead prediction $\hat{y}(t+h|t)$ can be calculated sequentially by using $h-1$ sample ahead prediction $\hat{y}(t+h-1|t)$. In this study, we have empirically set the parameters of SSA as: $N = 300, M = 250$ and $\tau = 18$.

4.3.2 Kernel Density Estimation (KDE) based method

A kernel density estimation (KDE) based prediction method is proposed in [13]. KDE is known as a non-parametric estimation of the probability density function (PDF). On KDE-based prediction method, the PDF by using the a-th covariate vector $x(t-k) = [y(t-h-k-(a-1)\delta), y(t-h-k-(a-2)\delta), \ldots, y(t-h-k)], k = 1,2,\ldots,K$ with lag length δ and its response $y(t)$ for specific prediction horizon h. Then the predicted value $\hat{y}(t+h|t)$ can be estimated as a mean of the conditioned probability distribution by the latest covariate vector $x(t)$. Designable parameters of KDE-based method are the dimension a of covariate vector, the lag length δ and the length for training sample K, respectively. In this study, we have used the parameters of KDE as: $a = 3$, $\delta = 15$, and $K = 300$.

4.3.3 Comparison results

SSA-based method and KDE-based method were tested their prediction performance on the same three data sets shown in figure 1.

Figure 10 shows the average MAEs of ZOH, SSA, and KDE and the proposed system with SVR. According to this comparison, the least MAE for all the prediction horizon $1 \leq h \leq 30$ was achieved by the proposed system with SVR. For $3 \leq h \leq 10$, SSA-based method achieved the second best MAE. However, MAE of SSA are the largest for $h \geq 15$ except MAE of ZOH. It is considered that SSA-based method is good for short- or mid-term prediction. KDE-based method showed relatively large MAE for small h, but achieved the second best MAE for $h \geq 14$. As seen above, the proposed method is superior to other prediction methods for the data sets tested.

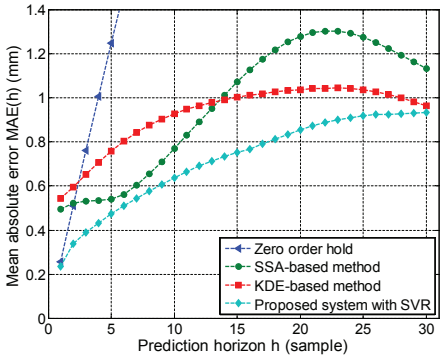

Figure 10. Mean absolute error MAE(h) with $\{t_s, t_e\} = \{1751, 3000\}$ for comparing the prediction performances of the proposed system with SVR and other prediction methods.

5 Conclusions

In this paper, a new lung tumor motion prediction system based on a time-varying SAR model was considered for accurate radiation therapy. The proposed method is composed of several different predictions including TVSAR model with different settings and a combination part to combining the predictions. It has been shown that the prediction performance of the proposed method with intelligent combinations of the useful pieces of information is basically superior to single predictions and clinically sufficient. Also according to the result of comparison with the state-of-the-art prediction methods, the proposed method achieved the best prediction performance.

Acknowledgments

The authors gratefully acknowledge Dr. Shirato and his colleagues at Hokkaido University Hospital for sharing tumor motion data. Also the authors thank Dr. Takai, Dr. Narita and their colleagues at Hirosaki University for their comments from the viewpoint of clinical medicine. A part of this study is financially supported by Varian Medical Systems, Inc. and Japan Society for the Promotion of Science (JSPS) KAKENHI Grant Numbers 25293258 and 11J08189.

References

[1] H. Onishi, T. Araki, H. Shirato, Y. Nagata, M. Hiraoka, K. Gomi, T. Yamashita, Y. Niibe, K. Karasawa, K. Hayakawa, Y. Takai, T. Kimura, Y. Hirokawa, A. Takeda, A. Ouchi, M. Hareyama, M. Kokubo, R. Hara, J. Itami, and K. Yamada, "Stereotactic hypofractionated high-dose irradiation for stage I nonsmall cell lung carcinoma: clinical outcomes in 245 subjects in a Japanese multiinstitutional study.," Cancer, vol. 101, Oct. 2004, pp. 1623-31.

[2] P.J. Keall, G.S. Mageras, J.M. Balter, R.S. Emery, K.M. Forster, S.B. Jiang, J.M. Kapatoes, D.a. Low, M.J. Murphy, B.R. Murray, C.R. Ramsey, M.B. Van Herk, S.S. Vedam, J.W. Wong, and E. Yorke, "The management of respiratory motion in radiation oncology report of AAPM Task Group 76.," Medical physics, vol. 33, 2006, pp. 3874-900.

[3] Hokkaido University Hospital, Sapporo, Japan. http://www.huhp.hokudai.ac.jp

[4] P.R. Poulsen, B. Cho, D. Ruan, A. Sawant, and P.J. Keall, "Dynamic multileaf collimator tracking of respiratory target motion based on a single kilovoltage imager during arc radiotherapy.," International Journal of Radiation Oncology, Biology, Physics, vol. 77, 2010, pp. 600-607.

[5] G.C. Sharp, S.B. Jiang, S. Shimizu, and H. Shirato, "Prediction of respiratory tumour motion for real-time image-guided radiotherapy," Physics in Medicine and Biology, vol. 49, 2004, pp. 425-440.

[6] D. Ruan and P. Keall, "Online prediction of respiratory motion: multidimensional processing with low-dimensional feature learning," Physics in Medicine and Biology, vol. 55, 2010, pp. 3011-3025.

[7] K. Ichiji, M. Sakai, N. Homma, Y. Takai, and M. Yoshizawa, "A Time Variant Seasonal ARIMA Model for Lung Tumor Motion Prediction," Proc. of The 15th Int'l Symposium on Artificial Life and Robotics 2010, 2010, pp. 485-488.

[8] K. Ichiji, M. Sakai, N. Homma, Y. Takai, and M. Yoshizawa, "SU-HH-BRB-10: Adaptive Seasonal Autoregressive Model Based Intrafractional Lung Tumor Motion Prediction for Continuously Irradiation," Medical Physics (Proc. of 52nd Annual Meeting of AAPM), vol. 37, 2010, pp. 3331-3332.

[9] N. Homma, M. Sakai, H. Endo, M, Mitsuya, Y. Takai, and M. Yoshizawa, "A New Motion Management Method for Lung Tumor Tracking Radiation Therapy," WSEAS Trans. Systems, Vol. 8, No. 4, 2009, pp.471-480.

[10] K. Ichiji, M. Sakai, N. Homma, Y. Takai, M. Yoshizawa, and H. Takeda, "Period Prediction of Lung Tumor Motion Time Series for Tracking Radiation Therapy," Proc. of SICE Tohoku-Chapter 45th Anniv. Workshop, 2009, pp. 23-26. (in Japanese)

[11] K. Ichiji, N. Homma, I. Bukovsky, M. Yoshizawa, "Intelligent sensing of biomedical signals — Lung tumor motion prediction for accurate radiotherapy," Merging Fields Of Computational Intelligence And Sensor Technology (CompSens), 2011 IEEE Workshop On, 2011, pp. 35-41. doi: 10.1109/MFCIST.2011.5949518

[12] C. Chang and C. Ling, "LIBSVM : a library for support vector machines," ACM Transactions on Intelligent Systems and Technology, 2:27:1–27:27, 2011. Software available at http://www.csie.ntu.edu.tw/~cjlin/libsvm

[13] D. Ruan, "Kernel density estimation-based real-time prediction for respiratory motion," Physics in Medicine and Biology, vol. 55, 2010, pp. 1311-1326.

[14] K. Demachi, H. Zhu, M. Ishikawa, and H. Shirato, "Predictive Simulation of tumor movement for Chasing Radiotherapy," Journal of the Japan Society of Applied Electromagnetics and Mechanics, vol. 17, 2009, pp. 222-226. (in Japanese)

[15] A. Mizuguchi, K. Demachi, and M. Uesaka, "Establish of the prediction system of chest skin motion with SSA method," International Journal of Applied Electromagnetics and Mechanics, vol.33, no. 3-4, 2010, pp. 1529-1533.

[16] D.W. Marquardt, "An algorithm for least-squares estimation of nonlinear parameters," Journal of the Society for Industrial & Applied Mathematics, vol. 11, 1963, pp. 431-441.

[17] C. M. Bishop, "Pattern recognition and machine learning," vol. 1. Springer New York, 2006.